TEMPORAL ANALYSIS OF ENVISAT'S ROTATIONAL MOTION

S. Sommer, J. Rosebrock, D. Cerutti-Maori, and L. Leushacke

Fraunhofer Institute for High Frequency Physics and Radar Techniques, Fraunhoferstraße 20, 53343 Wachtberg, Germany,
Email:svenja.sommer@fhr.fraunhofer.de

ABSTRACT

The Earth-observing satellite ENVISAT failed in April 2012 and orbits with an uncontrolled attitude. In order to remove ENVISAT from space in a potential de-orbiting mission, the attitude state of the satellite has to be known. We present attitude estimations using ISAR images obtained with the Tracking and Imaging Radar (TIRA) during 2011 - 2017. By matching wire grid models to the 2D ISAR images, the rotation vector can be estimated. After loss of contact, the spin period of ENVISAT decreased and reached the minimum in 2013. Since then, the spin period increased by $(75.0 \pm 0.9)\,\mathrm{ms\,d^{-1}}$ and reached $226\,\mathrm{s}$ in March 2017. An analysis of the rotation axis shows, that ENVISAT tumbles, where the rotation axis describes a nutation with a cone opening of about $80°$.

Key words: ISAR, image sequences, attitude estimation, rotational motion, ENVISAT.

1. INTRODUCTION

ENVISAT is one of the largest objects in orbit and the largest satellite launched by ESA. It is located in low earth orbit at $767\,\mathrm{km}$ and, therefore, in a highly populated orbit region. ENVISAT lost contact to ground stations in April 2012. After efforts to reestablish contact failed, ISAR images, among others, where used to determine the cause of the failure. ISAR images, together with photographic images from the French imaging satellite Pleiades, showed, that no external damages could be found. Still, ENVISAT is no longer controlled, meaning that it poses an increased danger to other satellites due to possible collision, especially in an orbit with a high density of objects.
Hence, ENVISAT is a possible target for a de-orbiting mission, where robotic satellites would capture ENVISAT and pull it into a reentry orbit. For such maneuver, the rotational velocity vector, i.e. rotation axis and angular velocity, of the satellite is essential to be known. Several studies have estimated EVISAT's attitude and spin velocities with various methods. Satellite laser ranging (SLR) and bi-static laser ranging were used to study ENVISAT's attitude [4, 8]. Ground based photometry was used by [3] and, additional to experimental studies, simulations have been performed to estimate the attitude of ENVISAT. [1] simulated the effects of Earth's gravity gradient and eddy currents. [7] used the softwaretool iOTA [2] to perform comparisons between modeling and SLR observations.
In this paper, we present estimations of the rotational motion of ENVISAT from 2011 - 2017 using 2D inverse synthetic aperture radar (ISAR) imaging with the Tracking and Imaging Radar (TIRA), operated by Fraunhofer FHR in Wachtberg, Germany. ISAR systems exploit the relative motion between the radar (which is usually stationary) and the object to be imaged (which is moving and/or rotating). Through its motion, the object is illuminated from different aspect angles. Radar echoes received from the object are coherently processed to gain 2D high resolution images.
Unlike optical instruments, the resolution of ISAR images is independent from range. Furthermore, radar systems are active systems and can be operated day and night. Another advantage compared to optical systems is the fact that radar systems are independent of the cloud coverage above the radar or other weather related restrictions. Hence, TIRA is an ideal instrument for space reconnaissance and for instance to observe (uncontrolled) satellites over long time periods to detect and estimate their rotational motion [6], that usually changes over time.

2. ISAR IMAGING OF SATELLITES

2.1. Principle

Radar measures the time delay between transmitting and receiving a radar pulse that is reflected at an object. That way, the range between radar and object is determined. To gain an image of the object, not only range information is necessary, but also information about the object structure perpendicular to range, the so-called cross-range. The range and cross-range span the image plane of an ISAR image. The cross-range can be estimated by

utilizing the motion between the radar and object. For satellite imaging, the radar is usually stationary on the Earth's surface while the satellite passes over the radar. The movement of the satellite and the radar during a pass is shown in Fig. 1.

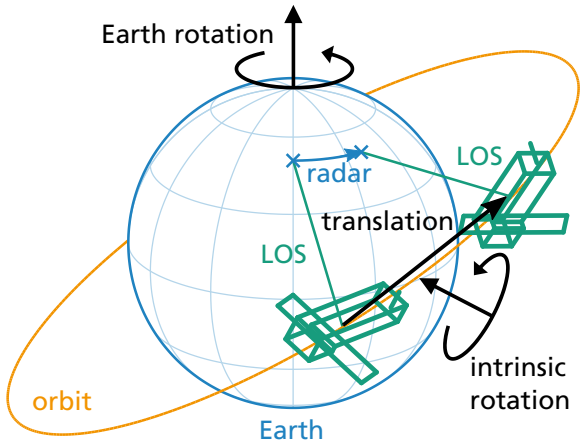

Figure 1. Observation geometry.

The coordinate system used in this paper is the Earth centered inertial (ECI) coordinate system if not stated otherwise. The x-axis points towards spring equinox, the z-axis is aligned with the Earth's spin axis and the y-axis is perpendicular to the aforementioned.
The motion of the satellite can be divided in two parts: translation and rotation. The translational motion is due to the orbital motion. The range variation from the radar to a salient point resulting from this motion and from Earth rotation needs to be compensated in order to gain ISAR images. The vector between the radar and object is called the line-of-sight (LOS) and changes while the satellite passes over the radar. The LOS direction relative to the satellite varies due to translational motion and Earth rotation but also due to a possible intrinsic rotation of the satellite. It is exploited to gain information about the object in cross-range as the relative distances between object points change between consecutive pulses causing corresponding phase changes. The effective rotation vector, responsible for the cross-scaling, is orthogonal to the plane spanned by the LOS moving relative to the satellite. It's norm, called rotation speed, is the angular velocity at which the LOS moves within its plane.

The rotation speed scales the cross-range of the ISAR image. That means, that the rotation affects the scaling of the object in cross-range. Hence, the rotation vector must be known a priori to estimate the cross-scaling of an ISAR image. Although radar location, orbit and Earth rotation are usually well known, the intrinsic motion of the object makes the cross-scaling of ISAR images hard to determine. The intrinsic rotation of the object is of great interest, but affects the cross-scaling of the ISAR images, which should be used to estimate the intrinsic rotation.

2.2. Attitude estimation

If the ISAR image planes and their scaling, relative to inertial coordinates, were known, the object's attitude could be estimated from its attitude relative to the image plane for every ISAR image. The attitude relative to the image plane can be determined by rotating a WGM (requiring that the objects dimensions are known) until its projection matches the ISAR image after appropriate cross-range scaling. Unfortunately, neither the image plane nor cross-scaling are known in advance.
To overcome the problem, the WGM is adapted manually to a set of ISAR images. Several WGM corners are assigned to the corresponding points in each ISAR image. In order to assess the validity of each assignment, it is useful to compare the assigned image points against the parallel projection of the rotated and cross-range scaled WGM. An example of two ISAR images of ENVISAT from the same pass are shown in Fig. 2. In both images, the image is centered around the main body, while the solar panel is partly cut off. The manually assigned WGM is shown in blue.

The next step is to estimate a rotation vector which fits all assigned points in the best way. This step assumes, that the rotation vector $\boldsymbol{\omega}$ is constant and does not change over the duration of the passage. If this assumption is not fulfilled, the passage can be divided in several sub-passage, where the assumption of a constant rotation vector can be upheld. The algorithm to determine the rotation vector is sketched in Fig. 3.

The initial attitude and rotation vector of the model are varied. Projections of the WGM corners, synthesized from these parameters, are then compared to the manually assigned points. The mean of squared distances ϵ between the them is used as an error measure. It can be calculated as

$$\epsilon^2 := \|\mathbf{R} - \mathbf{L}\mathbf{T}_0\mathbf{C}\|_F^2, \tag{1}$$

and depends on the matrix $\mathbf{L}$, which follows from $\boldsymbol{\omega}$ and contains the LOS unit vectors and their temporal derivatives (in a satellite-fixed coordinate system, which depends on the rotation vector). The initial attitude is defined by the matrix $\mathbf{T}_0$ which rotates the WGM coordinates contained in the columns of $\mathbf{C}$ to inertial coordinates at reference time. $\mathbf{R}$ contains range and range rate for different assigned images. The index F denotes the Frobenius norm, i.e. the square root of the sum of squares of all matrix entries.
By varying $\boldsymbol{\omega}$ and $\mathbf{T}_0$ to minimize ϵ^2, the optimal rotation vector and initial attitude for the assigned images can be determined.
The synthesized WGM projections resulting for the rotation vector for the example, shown in Fig. 2, are indicated in green and agree well with the manually assigned WGM projections (blue).

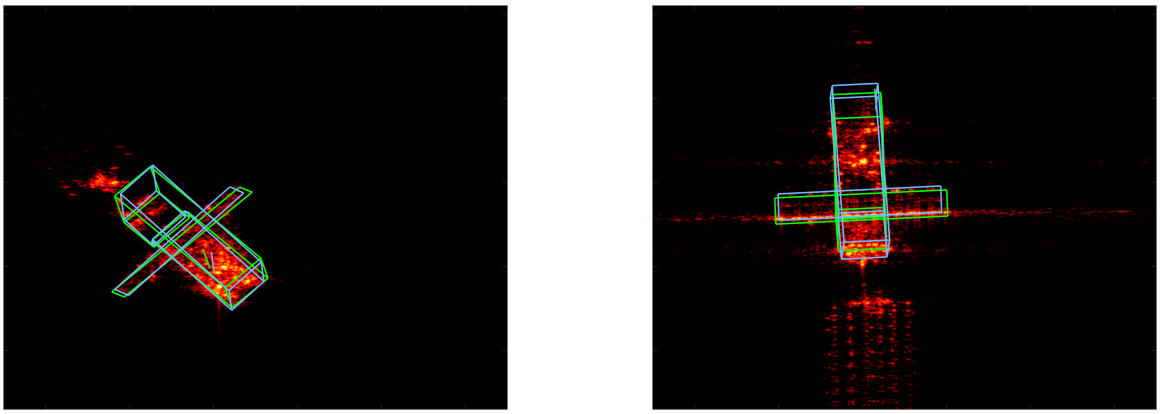

Figure 2. Two ISAR images of one passage with a manually assigned model (blue) and the projected WGM from the optimization (green).

3. LONG TERM OBSERVATIONS OF ENVISAT

ISAR observations of ENVISAT have been performed using the TIRA radar system. TIRA is located in Wachtberg, Germany (50.616°N, 7.126°E). It consists of an elevation-over-azimuth pedestal carrying a 34 m parabolic Cassegrain antenna, a narrowband L-band tracking radar and a broadband Ku-band imaging radar. For more details, see [5]. Here, the Ku-band imaging radar was used. It is a broadband coherent radar with a center frequency of 16.7 GHz with circular polarization. The 3 dB beam width is 0.031° with a typical peak power of 13 kW.

In this study, data from the years 2011 - 2017 (see Table 1 for exact dates) are used. The first observation of this series was conducted when ENVISAT was still active and in a stabilized attitude mode. Then, a series of observations have been performed shortly after the loss of contact on 8 April 2012 in order to assess possible external damage. Since, occasional observations have been performed from 2013 until March 2017, with an increase in observation during 2016/2017 to investigate the attitude motion in more detail.

No.	Start [UTC]	
1	29 Aug 2011	10:32:20
2	09 May 2012	10:19:20
3	23 May 2012	10:06:17
4	31 May 2012	11:51:58
5	08 Jan 2013	09:21:55
6	07 May 2013	09:57:07
7	25 Jul 2013	09:42:00
8	09 Oct 2013	09:43:50
9	21 Nov 2013	10:00:46
10	20 May 2015	09:50:05
11	07 Jun 2016	08:00:03
12	07 Jun 2016	08:04:55
13	06 Sep 2016	18:10:56
14	06 Sep 2016	19:48:19
15	21 Sep 2016	18:53:17
16	21 Sep 2016	20:32:18
17	11 Jan 2017	08:24:30
18	27 Jan 2017	10:10:08
19	22 Mar 2017	08:30:08

Table 1. TIRA observation dates of ENVISAT

3.1. Rotation velocity, spin period

The rotation velocity is the magnitude of the rotation vector in the inertial frame of reference (ECI coordinates, *J2000*). Before loss of contact, ENVISAT orbited Earth in a gravitational stabilized attitude, i.e., the same part of the satellite pointed towards Earth's center during an orbit [4]. This rotation corresponds to a rotation velocity of about $0.06\,^\circ\,\mathrm{s}^{-1}$ in the inertial frame of reference. Indeed, we estimated a rotation velocity of $0.06\,^\circ\,\mathrm{s}^{-1}$ before the loss of contact, which is in good agreement with the actual rotation velocity.

The estimated rotation velocity of all observations are presented in Fig. 4. After the loss of contact, the rota-

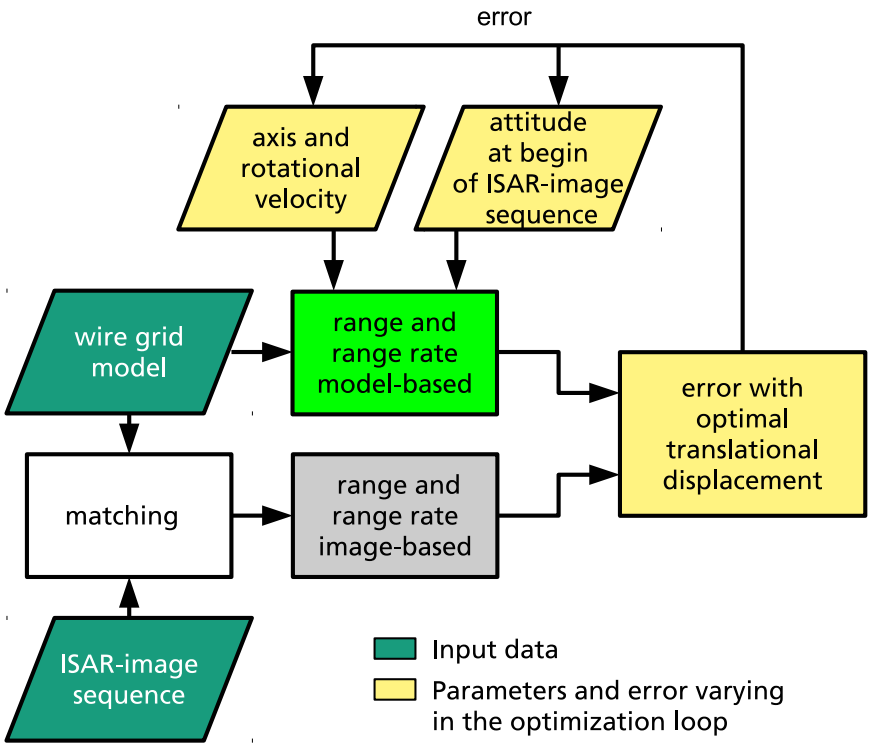

Figure 3. Algorithm outline.

tion velocity increased from April 2012 until May 2013. In May 2013, the highest rotation velocity was estimated to be to $2.9\,^\circ\,\mathrm{s}^{-1}$, corresponding to a spin period of $124\,\mathrm{s}$. The actual rotation velocity might have been higher, but cannot be resolved here due to the limited numbers of observations at that time.

The spin period (inverse of rotation velocity) is regarded separately in Fig. 5 as the temporal development of the spin period might be of interest for possible deorbiting missions. The spin period between May 2013 and March 2017 was fitted, depending on time, with a linear regression of the form $y = mx + n$ (red) and $\ln(y) = a + bx$ (blue). It can be found that the linear fit (correlation coefficient 0.996) fits the data better than an exponential fit (correlation coefficient 0.989). The estimated linear fit of the spin periods depending on time is described by

$$y = (0.0750 \pm 0.0009)\,\mathrm{s\,d}^{-1} \cdot D + (115.0 \pm 0.9)\,\mathrm{s}, \quad (2)$$

where D is the number of days since 1 January 2013. Hence, we estimate that the spin period of ENVISAT seems to increase with $(75.0 \pm 0.9)\,\mathrm{ms}$ per day.

Additional to our data, Fig. 5 shows also fits from two other studies. The green line is based on the study by [4] who collected data during 2013 using satellite laser ranging and used a linear fit. The dashed green lines indicate the possible temporal development extrapolated from their fit. Although their spin period estimation for 2013 does not deviate much from our estimation in 2013, the extrapolated values differ widely for later years.
A study by [3], indicated by the cyan line, using photometry with data from 2013 to 2015, found a quadratic fit for their results. Their measurements are, in the first approximation, in good agreement with our results, although there are differences especially in the begin and end of our observation period. For 2013, their fit tends to overestimate the spin period slightly compared to our results, and the extrapolated seems to overestimate the spin period even more strongly.

An overview of the results from this study as well as from [4] and [3] is given in Table 2. Our estimations for the minimum spin velocity correspond well to the measurements of [4] in the way that the spin period decreases after the loss of contact until around April/May 2013.
After that, the rotation velocity begins to decrease. The rotation period of ENVISAT is found to increase linearly with $(75.0 \pm 0.9)\,\mathrm{ms\,d}^{-1}$, while [4] estimated an increase in spin period of $36.7\,\mathrm{ms\,d}^{-1}$. [3] estimated a spin period increase of $57\,\mathrm{ms\,d}^{-1}$ for 2013, and based on their fit function, an increase of $104.4\,\mathrm{ms\,d}^{-1}$ on average for 2016. Although our linear fit corresponds fairly well with the quadratic fit of [3] with small deviations, the fit of [4] shows a far smaller increase in spin period duration. A major reason for this might be the different observation periods. [4] used observations from 2013, while [3] used data from 2013 - 2015 and this study data from 2013 to 2017 for the trend analysis of the spin

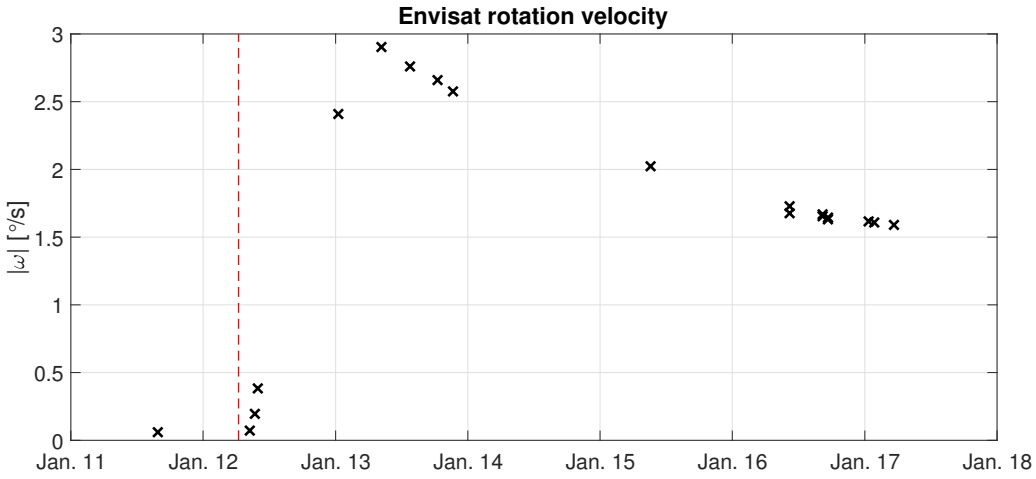

Figure 4. Angular velocity derived by TIRA measurements from August 2011 to March 2017. The red dashed line indicates the date of loss of contact, 8 April 2012.

Study	minimum spin period	spin period increase 2013	spin period increase 2016	degree of polynomial fit
Sommer et al., 2017	124 ms	75.0 ms d^{-1}	75 ms d^{-1}	1
Kucharski et al., 2014	128 ms	36.7 ms d^{-1}	36.7 ms d^{-1}	1
Koshkin et al., 2016	-	57 ms d^{-1}	104.4 ms d^{-1} (average)	2

Table 2. Comparison to other studies

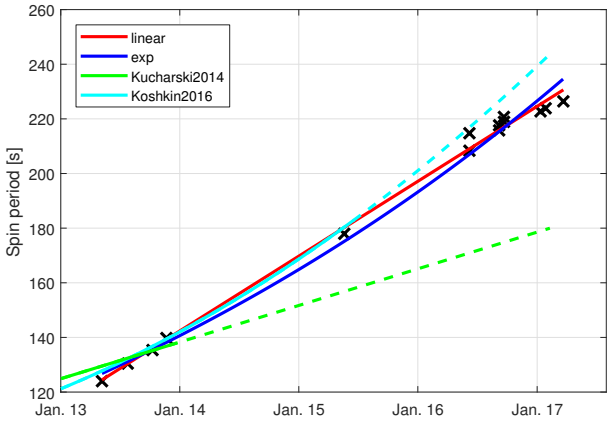

Figure 5. Estimated spin periods. The red line is a linear regression of the data obtained with TIRA, the blue an exponential fit. The cyan line indicates the fit of the spin period obtained by [3] and the green line by [4].

period.

3.2. Spin period prediction performance

To investigate the prediction performance of spin period estimations using ISAR images, we fitted spin periods for two different time periods in the past and compared the extrapolated spin periods to recent observations. The first set of spin periods is from 2013 (observation No. 6 - 9). The linear fit of the spin periods is shown in Fig. 6 in dark blue. The light blue area indicates the confidence interval of the fit using the 0.95-quantile of Student's t-distribution.

The next set of spin periods uses data from 2013 and 2015 (observation no. 6 - 10). The linear fit is indicated in Fig. 6 by the dark green line, the corresponding extrapolation by the dashed dark green line. The light green area indicates the confidence interval of the corresponding fit using the 0.95-quantile of Student's t-distribution. The linear fit taking all data since May 2013 into account is indicated by the red line. No uncertainty is shown for this fit as no prediction was made using all data. For the uncertainty of this fit, see above.

Comparing the extrapolated values from the first time period (2013) to the actual data, it can be seen, that the extrapolation agrees quite well with observations taken in 2016/2017. All estimated spin velocities lie within the uncertainty of the fit. Taking the observation from 2015 also into account shows that the slope of this fit is smaller than for the first fit, but still, the extrapolated values agree, within the uncertainty, with observed values from 2016/2017. Comparing both extrapolated fits to the linear fit of all data (red line) shows that the red line lies between both extrapolated fits and within the areas of uncertainty. Hence, the extrapolated values are in good agreement with the actual measurements. The prediction performance of radar using ISAR imaging should be compared to model simulations in future studies.

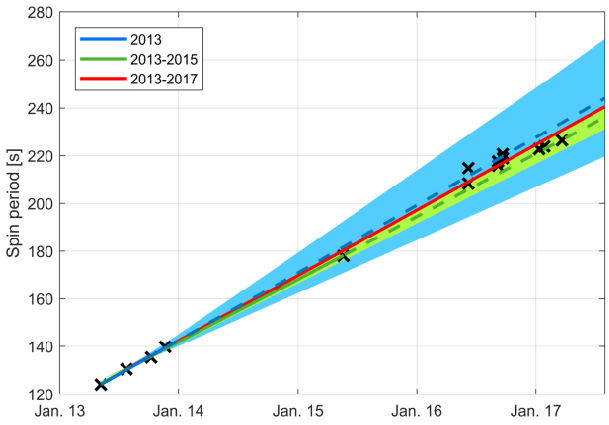

Figure 6. Prediction performance of spin period estimates of ISAR imaging with TIRA. The dark blue line indicates a linear fit to data from 2013, the dark green line a linear fit to data from 2013/2015 and the red line to all data (May 2013 - March 2017). The light blue and light green areas indicate the confidence interval of the fits.

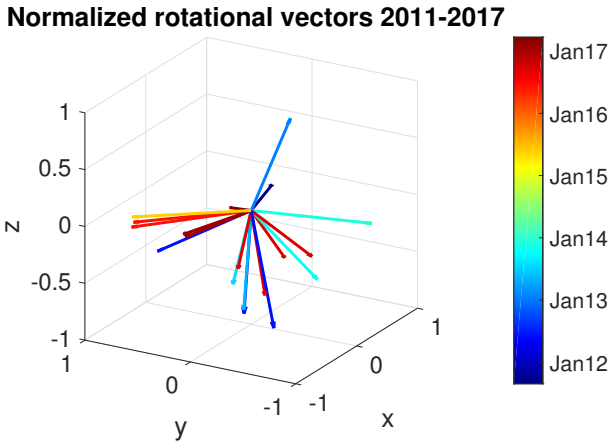

Figure 7. Normalized velocity vectors in inertial coordinates (ECI), August 2011 - January 2017

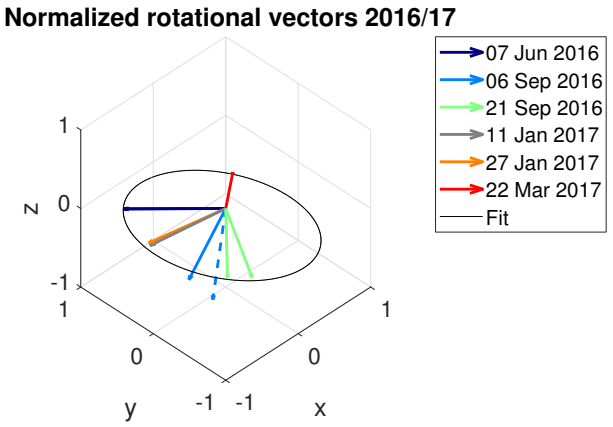

Figure 8. Normalized velocity vectors, July 2016 - January 2017, fitted with a cone. The dashed line indicates an outlier and was omitted for the fit.

3.3. Spin axis

Additonally to the rotation velocity estimations, we derived the spin axis of ENVISAT. The different spin axes of ENVISAT, i. e. the normalized rotational vectors in an inertial frame of reference, are shown in Fig. 7 for 2011 - 2017. The temporal evolution is color coded. The first two years after loss of contact (2012/2013, bluish colors) do not show a distinct direction for the rotational axis. This might indicate that ENVISAT made a tumbling movement, meaning the rotational axis is not constant in the inertial frame of reference.

On the other hand, the spin axes for the years 2016/2017 show a more coherent pattern. This is examined in detail in Fig. 8. Here, we show the rotational axis only for the observations in 2016/2017. The rotation axis varies over time, but it can be seen that the rotation axis for two measurements of the same day show almost in the same direction. Additionally, the vectors appear to lie roughly on a cone, therefore we fitted a cone to the data but omitted an outlier (6 September 2016, 18:10:56). The result is indicated by the black circle in Fig. 8. The resulting cone opening is about $80°$ and the normalized cone axis points towards $[-0.22; 0.02; -0.97]$. Although there are some deviations from the fitted cone, the results indicate that the rotational axis is not fixed and ENVISAT performs a nutation. Comparing the variances of the rotation axes in 2013 and 2016/2017, it seems that the tumbling movement decreased, but ENVISAT still tumbles.

On the other hand, [4] found that the spin vector is almost perpendicular to the along-track vector in 2013. [3] found that ENVISAT appears to be spinning around an axis parallel to the normal of the orbit. The analysis of [4] relies on assumption that the spin axis of ENVISAT is stable from 10 April to 25 September 2013. During this period, we analyzed two passages, on 07 May and 25 July 2013. The angle between rotation axes on those dates, as they have been estimated using ISAR in conjunction with a WGM, is $17.6°$. Hence, ISAR imaging provides the means to estimate the rotation velocity without the assumption of a long-term stable rotation axis. On the other hand, this method assumes that the rotation axis is constant for the duration of a passage. In case of fast tumbling objects, this might not be the case but can be overcome by dividing a passage in different subpassages, where the assumption of a fixed rotation axis is reasonable. In the case for this ENVISAT study, the tumbling movement is slow, meaning that the assumption of a fixed rotation vector can be upheld for one pass.

4. CONCLUSION

The attitude of a space object can be determined by ISAR imaging in conjunction with wire grid models. This method can be used for long term studies of the attitude of uncontrolled space objects, in this case, ENVISAT. The increase in spin period with time, which was found in this study, can also be used to make simple extrapolations of future spin periods, assuming a linear trend as found in this study. It was shown, that the extrapolated values from short periods of time fit quite well to later observations. Additionally, ISAR imaging can be used to determine the rotation axis of an object. In the case of ENVISAT, it appears that it tumbles with a nutation. These informations might be helpful for a potential deorbiting mission of ENVISAT. In order to verify the linear trend in the spin period, additional observations should be conducted in the future.

REFERENCES

1. Natalia Ortiz Gómez and Scott J.I. Walker. Earth's gravity gradient and eddy currents effects on the rotational dynamics of space debris objects: Envisat case study. *Advances in Space Research*, 56(3):494–508, August 2015. doi: 10.1016/j.asr.2014.12.031.
2. R. Kanzler, T. Schildknecht, T. Lips, B. Fritsche, J. Silha, and H. Krag. Space debris attitude simulation - iota (in-orbit tumbling analysis). In *Advanced Maui Optical and Space Surveillance Technologies Conference*, page 33, 2015.
3. N. Koshkin, E. Korobeynikova, L. Shakun, S. Strakhova, and Z.H. Tang. Remote sensing of the EnviSat and cbers-2B satellites rotation around the centre of mass by photometry. *Advances in Space Research*, 58(3):358–371, August 2016. doi: 10.1016/j.asr.2016.04.024.
4. D. Kucharski, G. Kirchner, F. Koidl, C. Fan, R. Carman, C. Moore, A. Dmytrotsa, M. Ploner, G. Bianco, M. Medvedskij, A. Makeyev, G. Appleby, M. Suzuki, J. M. Torre, Z. Zhongping, L. Grunwaldt, and Q. Feng. Attitude and Spin Period of Space Debris Envisat Measured by Satellite Laser Ranging. *IEEE Transactions on Geoscience and Remote Sensing*, 52(12): 7651–7657, Dec 2014. ISSN 0196-2892. doi: 10.1109/TGRS.2014.2316138.
5. D. Mehrholz. Ein Verfolgungs- und Abbildungsradarsystem zur Beobachtung von Weltraumobjekten. *Frequenz*, 50:138–146, July 1996. doi: 10.1515/FREQ.1996.50.7-8.138.
6. J. Rosebrock. Absolute attitude from monostatic radar measurements of rotating objects. *IEEE Transactions on Geoscience and Remote Sensing*, 49(10): 3737–3744, October 2011. ISSN 0196-2892. doi: 10.1109/TGRS.2011.2159727.
7. J. Silha, T. Schildknecht, J. Pittet, D. Bodenmann, R. Kanzler, P. Karrang, and H. Krag. Comparison of ENVISAT's Attitude Simulation and Real Optical and SLR Observations in order to Refine the Satellite Attitude Model. In S. Ryan, editor, *Advanced Maui Optical and Space Surveillance Technologies Conference*, page 54, September 2016.
8. H. Wirnsberger, O. Baur, and G. Kirchner. Space debris orbit prediction errors using bi-static laser observations. Case study: ENVISAT. *Advances in Space Research*, 55:2607–2615, June 2015. doi: 10.1016/j.asr.2015.02.018.